JACS
JOURNAL OF THE AMERICAN CHEMICAL SOCIETY
Article
pubs.acs.org/JACS

Carrier Generation in Multicomponent Wide-Bandgap Oxides: $InGaZnO_4$

Altynbek Murat,[†] Alexander U. Adler,[‡] Thomas O. Mason,[‡] and Julia E. Medvedeva*,[†]

[†]Department of Physics, Missouri University of Science & Technology, Rolla, Missouri 65409, United States
[‡]Department of Materials Science and Engineering, Northwestern University, Evanston, Illinois 60208, United States

ABSTRACT: To exploit the full potential of multicomponent wide-bandgap oxides, an in-depth understanding of the complex defect chemistry and of the role played by the constituent oxides is required. In this work, thorough theoretical and experimental investigations are combined in order to explain the carrier generation and transport in crystalline $InGaZnO_4$. Using first-principles density functional approach, we calculate the formation energies and transition levels of possible acceptor and donor point defects as well as the implied defect complexes in $InGaZnO_4$ and determine the equilibrium defect and electron densities as a function of growth temperature and oxygen partial pressure. An excellent agreement of the theoretical results with our Brouwer analysis of the bulk electrical measurements for $InGaZnO_4$ establishes the Ga antisite defect, Ga_{Zn}, as the major electron donor in $InGaZnO_4$. Moreover, we show that the oxygen vacancies, long believed to be the carrier source in this oxide, are scarce. The proposed carrier generation mechanism also explains the observed intriguing behavior of the conductivity in In-rich vs Ga-rich $InGaZnO_4$.

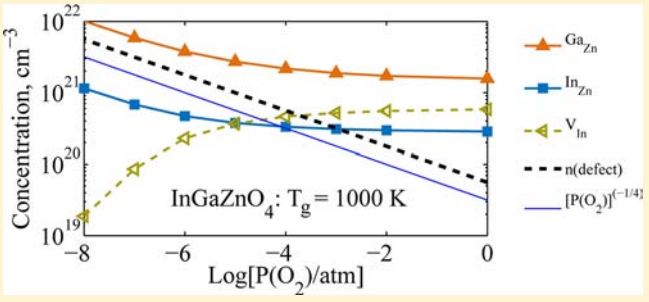

1. INTRODUCTION

One of the major challenges in the area of transparent conducting and semiconducting oxides[1−11] concerns understanding the defect/doping mechanism(s) responsible for carrier generation in these wide-bandgap materials. Strikingly, despite a substantial theoretical development,[12−21] the origin of the conductivity in the well-known and commercially most widely used transparent conducting oxide, Sn-doped In_2O_3 or ITO, and particularly the competition between intrinsic defects (oxygen and cation vacancies and interstitials) and cation substitutional dopants (Sn on In sites), has been clarified only recently.[22,23] But for the ternary and quaternary oxides the situation remains unclear. The structural and compositional complexity of these multi-cation materials—although they are highly appealing technologically due to the possibility of controlling the electrical, optical, and thermal properties over wide ranges—requires in-depth understanding of the complex defect chemistry in order to determine the carrier source(s). In addition to multiple cations' vacancies and interstitials, possible donor and acceptor defects also include cation antisites, such as Ga_{Zn}, Zn_{In}, etc. Several of these defects may coexist or compete under varying growth conditions owing to the similarities of the metal−oxygen bond strengths of the oxide constituents. Moreover, a layered structure and/or a distinct cation order in crystalline multicomponent oxides may favor specific defect distributions and formation of defect complexes.

For the homologous compounds $(In,Ga)_2O_3(ZnO)_n$, with n = integer, a widely studied and technologically important series of multicomponent oxides,[24−32] neither the origin of the conductivity nor the role played by each constituent oxide in the defect formation has been established. It is commonly believed[24] that oxygen vacancies are the carrier source in complex $(In,Ga)_2O_3(ZnO)_n$ due to the high sensitivity of the electrical properties to the oxygen partial pressure, pO_2, during pulsed laser deposition of amorphous In-Ga-Zn-O (IGZO) films[33] and shallow oxygen vacancy defects for some local structure configurations in amorphous $InGaZnO_4$.[34,35] However, first-principles investigations of crystalline non-stoichiometric $InGaZnO_4$ (n = 1) showed that oxygen vacancies cannot explain the observed conducting behavior in this material because they form at a deep level within the band gap.[36−38]

Furthermore, in bulk crystalline samples of IGZO (n = 1, 2, 3) measured by Moriga et al., conductivity is enhanced approximately an order of magnitude by a reductive anneal in forming gas (4% H_2, balance N_2). However, with an increase in In:Ga ratio, conductivity increases as much as 3 orders of magnitude (for example, when [In]/([In]+[Ga]) varies from 0.25 to 1.0 in n = 3 IGZO).[26] This suggests that the dominating defect mechanism for crystalline IGZO involves more than just oxygen defect concentrations and, indeed, may involve cation defects. It should also be pointed out that, in Ga-free $In_2O_3(ZnO)_3$, indium antisite donors (In_{Zn}) were found to be shallow donors with a low formation energy comparable to that of the oxygen vacancy.[39]

Received: December 7, 2012
Published: March 13, 2013

   dx.doi.org/10.1021/ja311955g | J. Am. Chem. Soc. 2013, 135, 5685−5692

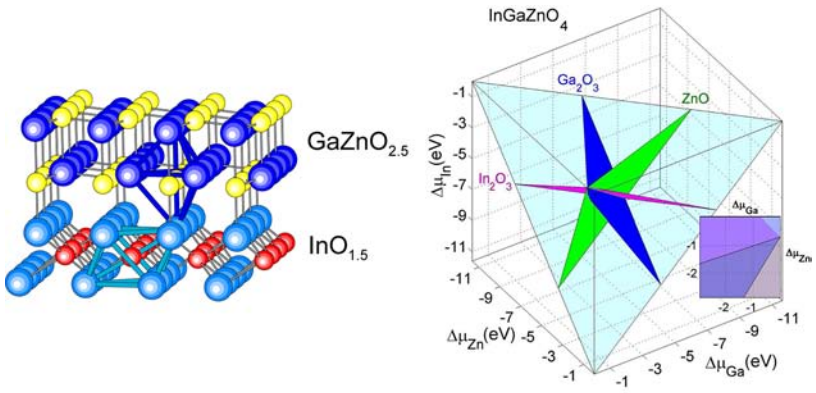

Figure 1. (Left) The crystal structure of $InGaZnO_4$ consists of alternating layers of six-fold coordinated In atoms and five-fold coordinated Ga and Zn atoms distributed randomly. (Right) Available elemental chemical potentials for $InGaZnO_4$. Shaded planes represent the stability of the corresponding binary phases. The inset shows the extreme metal-rich values ($\Delta\mu_{In} = 0$).

In this work, we combine the results of the Brouwer analysis of bulk electrical measurements in crystalline $InGaZnO_4$ with thorough first-principles investigations of the donor and acceptor defects in this multicomponent oxide in order to determine the leading electron donor and to elucidate the intriguing conductivity behavior in IGZO.

2. THEORETICAL METHODS

First-principles full-potential linearized augmented plane wave methods[40,41] with the local density approximation (LDA) and the screened-exchanged LDA[42−46] are employed for accurate energy and electronic band structure calculations. Cutoffs for the basis functions, 16.0 Ry, and potential representation, 81.0 Ry, and expansion in terms of spherical harmonics with $l \leq 8$ inside the muffin-tin spheres were used. Summations over the Brillouin zone were carried out using at least 23 special **k** points in the irreducible wedge.

$InGaZnO_4$ has the rhombohedral ($R\bar{3}m$) layered crystal structure, in which two chemically and structurally distinct layers—$InO_{1.5}$ with six-fold-coordinated In atoms and $GaZnO_{2.5}$ with five-fold-coordinated randomly distributed Ga and Zn atoms—alternate along the [0001] direction.[47−50] The optimized internal atomic positions for undoped stoichiometric $InGaZnO_4$ have been reported earlier.[37,51,52] In this work, we consider both donor and acceptor native defects in $InGaZnO_4$: cation and anion vacancies or interstitials as well as antisite defects, Ga_{Zn}, In_{Zn}, Zn_{Ga}, and Zn_{In}. For this, a 49-atom supercell was used with the lattice vectors $(30\bar{2})$, $(\bar{1}12)$, and $(02\bar{1})$, given in the units of the rhombohedral primitive cell vectors. For every structure investigated, the internal positions of all atoms were optimized via the total energy and atomic forces minimization.

The formation energy of a defect in a charge state q, which is modeled using a corresponding background charge, is a function of the Fermi level and the corresponding chemical potential:

$$\Delta H(E_F, \mu) = E_{defect} - E_{host} \pm \mu_\alpha + q(E_F) \quad (1)$$

Here, E_{defect} and E_{host} are the calculated total energies for the oxide with the defect and the stoichiometric oxide in the same size supercell, respectively; μ_α is the chemical potential of an atom added to (−) or removed from (+) the lattice; q is the defect charge state; E_F is the Fermi energy taken with respect to the top of the valence band. The chemical potential $\mu_\alpha = \mu_\alpha^0 + \Delta\mu_\alpha$ is taken with respect to the chemical potential μ_α^0 of the elementary bulk metals (orthorhombic Ga, tetragonal In, and hexagonal Zn) or the O_2 molecule. The deviation from the elemental chemical potential, $\Delta\mu_\alpha$, is determined by the thermal stability conditions of the host:

$$\Delta\mu_{In} + \Delta\mu_{Ga} + \Delta\mu_{Zn} + 4\Delta\mu_O = \Delta H_f[InGaZnO_4] \quad (2)$$

To avoid precipitation of the elements and formation of the secondary-phase binary oxides, the following conditions must be satisfied:

$$\Delta\mu_{In} \leq 0; \quad \Delta\mu_{Ga} \leq 0; \quad \Delta\mu_{Zn} \leq 0; \quad \Delta\mu_O \leq 0 \quad (3)$$

$$2\Delta\mu_{In} + 3\Delta\mu_O \leq \Delta H_f(In_2O_3) \quad (4)$$

$$2\Delta\mu_{Ga} + 3\Delta\mu_O \leq \Delta H_f(Ga_2O_3) \quad (5)$$

$$\Delta\mu_{Zn} + \Delta\mu_O \leq \Delta H_f(ZnO) \quad (6)$$

Hence, the available range for the elemental chemical potentials in the case of quaternary $InGaZnO_4$ is a three-dimensional volume determined by the above stability conditions (eqs 4−6), projected onto the corresponding $InGaZnO_4$ plot (eq 2).

The heat of formation, ΔH_f, for the oxides is calculated with respect to the bulk orthorhombic Ga, tetragonal In, and hexagonal Zn. The ΔH_f value for $InGaZnO_4$ is found to be −11.28 eV. Calculating the corresponding heat of formation for the binary constituents, we find that

$$2\Delta H_f[InGaZnO_4] > \Delta H_f(In_2O_3) + \Delta H_f(Ga_2O_3) + 2\Delta H_f(ZnO) \quad (7)$$

The above equation suggests that, at zero temperature, the formation of $InGaZnO_4$ is impossible without the formation of the corresponding binary phases. This also means that there are no available elemental chemical potentials which would allow the formation of the multicomponent oxide. Since the latter is stable above 1000 K,[47−49] the entropy term $T\Delta S$ must be taken into consideration. Similar arguments were reported for $In_2O_3(ZnO)_k$ compounds.[39] The entropy term can be estimated on the basis of the equilibrium solid-state reaction which involves the binary constituents as follows:

$$\Delta H_f[InGaZnO_4] - \frac{1}{2}[\Delta H_f(In_2O_3) + \Delta H_f(Ga_2O_3) + 2\Delta H_f(ZnO)] = T_{InGaZnO_4}\delta S_{InGaZnO_4} \quad (8)$$

We then replace the ΔH_f for $InGaZnO_4$ with the obtained $[\Delta H_f - T\delta S]$ in eq 2 above. As a result, a very narrow range of the available elemental chemical potentials for secondary-phase-free $InGaZnO_4$ exists along the crossing line of the three planes (eqs 4−6, Figure 1). This is in accord with the results for Ga-free layered multicomponent $In_2O_3(ZnO)_3$.[39]

The dependence of $\Delta\mu_O$ on the growth conditions, i.e., temperature and oxygen partial pressure pO_2, is considered according to ref 53

dx.doi.org/10.1021/ja311955g | J. Am. Chem. Soc. 2013, 135, 5685−5692

using the tabulated enthalpy and entropy values for the O_2 gas at T = 298 K and P = 1 atm. We also take into account that the band gap E_g decreases with temperature at a rate of about 0.32 meV/K as observed in our experiments. Our screened-exchange LDA-calculated band gap in stoichiometric $InGaZnO_4$ is found to be 3.29 eV, which is in excellent agreement with the one measured at 300 K, 3.34 eV.

In addition to the band-gap correction via the screened-exchanged LDA method,[42] we also address the band-edge and the finite-size supercell errors in the defect calculations. We employ the correction methods proposed by Lany and Zunger,[22,54] namely, (i) shifting of shallow levels with the corresponding band edges of the host; (ii) band-filling correction; (iii) potential-alignment correction for supercells with charged defects; and (iv) image charge correction for charged defects via simplified Makov–Payne scheme.[54] For the latter one, we used the static dielectric constant of 8.98, which is a volume-fraction average of the dielectric constants of ZnO, In_2O_3, and Ga_2O_3 as follows from the Maxwell–Garnett effective medium theory.[55]

Once the formation energies of the donor and acceptor defects in $InGaZnO_4$ are obtained, we calculate the defect and carrier concentrations, $n(E_F,\mu,T) = N_{sites}\exp(-\Delta H(E_F,\mu)/kT)$, at the *equilibrium* Fermi level, which is determined by the charge neutrality condition that accounts for all the carriers and ionized defects in $InGaZnO_4$ grown under equilibrium conditions.[22,53] N_{sites} is the number of available sites for a particular defect in the lattice per volume, k is the Boltzmann constant, and T is the temperature.

3. EXPERIMENTAL METHODS

Bulk polycrystalline pellets were prepared from ZnO, In_2O_3 (both >99.99% purity, cation basis, Alfa Aesar, Ward Hill, MA), and Ga_2O_3 (>99.99% purity, cation basis Aldrich Chemical Co., Milwaukee, WI). The dried starting powders were ground under acetone in an agate mortar and pestle. The pellets were calcined at 1000 °C overnight and reground. The dry powder was then pressed into half-inch-diameter pellets at 120 MPa, sintered at 1350 °C for 48 h, and quenched in air. The pellets were embedded in sacrificial powder and nested in a series of alumina crucibles in order to mitigate volatilization of Zn, and weight loss during firing averaged less than 0.7%. Phase purity was verified via X-ray diffraction on a Rigaku Geigerflex diffractometer (Rigaku Inc.) with a Cu Kα source both before and after the *in situ* experiments described below.

The fractional porosity (ϕ) of the specimens varied from 0.25 to 0.35, so a correction from measured conductivity (σ_m) to true conductivity (σ_t) is necessary.[56] Measured conductivities were corrected to true conductivities using the Bruggeman asymmetric equation,[57]

$$\sigma_t(\phi) = \frac{\sigma_m}{1 - \frac{3}{2}\phi} \tag{9}$$

It should be stressed that since density was found not to change during the course of the 750 °C electrical measurements, this correction does not play a role in the slope obtained by Brouwer analysis described below.

Ceramic bars were cut from the sintered pellets with a low-speed diamond saw. Bars of dimensions 4.27 × 2.74 × 9.17 mm (W×H×L) were mounted in four-point linear geometry in an alumina sample holder between two gold foil plates attached to two type-S thermocouple beads which doubled as current leads and wrapped at approximately one-fourth and three-fourths the length of the bar with gold wire attached to two type-S thermocouples which doubled as voltage leads for thermopower measurements as described in ref 58. Mounted bar-shaped samples were placed in a sealed quartz tube, and commercial mixtures of O_2 gas balanced with Ar (with pO_2 ranging from 100 ppm to 20%) were introduced. Oxygen partial pressure in the sealed tube furnace was monitored by a zirconia oxygen cell, and a computer-controlled scanner (model 705), current source (model 224), and digital multimeter (model 196) were used to simultaneously measure the conductivity and thermopower *in situ* (Kiethley Instruments, Cleveland, OH). Equilibrium was considered to have been reached when the rate of change in the conductivity values was less than approximately 1% per day and typically took 5–8 days to reach.

3.1. Brouwer Analysis of Bulk Electrical Measurements. The well-known process of "Brouwer analysis" was applied to the data collected by *in situ*/equilibrium electrical property measurements. In Brouwer analysis, the data are plotted as log–log plots of either electrical conductivity or modified Seebeck coefficient vs oxygen partial pressure. Since the electrical conductivity (σ) of a non-degenerate n-type semiconductor is given by

$$\sigma = ne\mu \tag{10}$$

where e is the elementary charge of an electron and μ is the charge carrier mobility, if we assume that the latter (mobility) is independent of pO_2 over the narrow range of values employed in the present work (10^{-5}–10^{-1}), we arrive at the relationship

$$\log(\sigma) = \log(n) + \text{Const.} \tag{11}$$

$$\log(\sigma) \propto \log(n) \tag{12}$$

Similarly, for a non-degenerate n-type semiconductor-doped semiconductor, the Seebeck coefficient or thermopower is given by

$$Q = -\frac{k}{e}\left[\ln\frac{N_C}{n} + A\right] = \frac{k}{e}[\ln(n) - \ln(N_C) - A] \tag{13}$$

where k is the Boltzmann constant, N_C is the effective density of states in the conduction band, and A is the constant (entropy of transport) that depends upon the scattering mechanism. If we assume that both N_C and A are invariant with pO_2 over the narrow range of values studied, we arrive at a modified Seebeck coefficient:

$$\frac{Q}{2.303(k/e)} = Q_{red} = \log(n) - \text{Const.} \tag{14}$$

$$\frac{Q_{red}}{2.303} \propto \log(n) \tag{15}$$

If the above assumptions prove valid, the only variable on the right side of eqs 11 and 14 is the electron population; both properties should exhibit the identical log–log dependence upon carrier content, and therefore upon oxygen partial pressure. This is the basis of Brouwer analysis for which results are described later.

4. THEORETICAL RESULTS

4.1. Defect Calculations from First Principles. In our theoretical studies, we consider the electron donors (oxygen vacancies; Zn, Ga, and In interstitials; Ga_{Zn} and In_{Zn} antisites) and the electron "killers" (oxygen interstitial; Zn, Ga and In vacancies; Zn_{Ga} and Zn_{In} antisites), as well as neutral Ga_{In} and In_{Ga} antisites. In addition, we calculate the formation of a $Ga_{Zn}V_{In}$ complex which combines the major donor and acceptor point defects.

Owing to the layered structure of $InGaZnO_4$, cf. Figure 1, several intrinsic defects may have a distinct distribution within the lattice. In particular, we calculated six nonequivalent site locations for an oxygen vacancy,[59] nine site locations for an interstitial oxygen,[37] and three site locations for In_{Zn} and Ga_{Zn} antisites; all site locations have the same five-fold oxygen coordination but different sets of the next-nearest-neighbor atoms, namely, 6Ga3Zn, 5Ga4Zn, and 4Ga5Zn. We find that (i) the formation energies of an oxygen vacancy located in the $InO_{1.5}$ layer and in the $GaZnO_{2.5}$ double layer are nearly identical, giving rise to a uniform distribution of the oxygen defect throughout the layered structure of $InGaZnO_4$;[59] (ii) the most energetically preferable location for an oxygen interstitial atom is slightly above the $InO_{1.5}$ layer[37] and at the distance of 2.14 and 1.87 Å from In and Ga atoms, respectively; and (iii) both Ga_{Zn} and In_{Zn} defects prefer the site location with the

dx.doi.org/10.1021/ja311955g | J. Am. Chem. Soc. 2013, 135, 5685–5692

largest number of Zn neighbor atoms, i.e., 4Ga5Zn (which is in accord with the random distribution of the Ga^{3+} and Zn^{2+} atoms in the $GaZnO_{2.5}$ layers as opposed to segregation).

Figure 2 shows the calculated formation energies of the donor and acceptor defects as a function of the Fermi level for

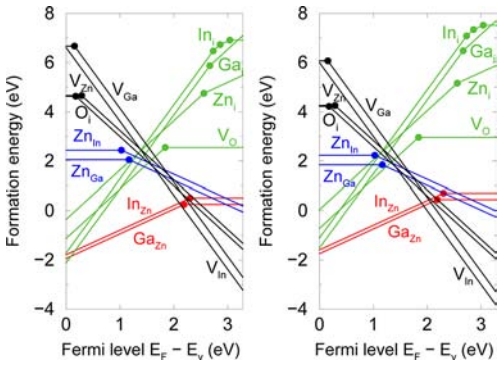

Figure 2. Calculated formation energies ΔH_f (eq 1) of donor and acceptor defects in $InGaZnO_4$ at growth temperature T = 1023 K as a function of the Fermi level with respect to the top of the valence band E_v. The dots represent the transition energies between different charge states. (a) In the metal-rich conditions, oxygen partial pressure pO_2 = 0.0001 atm, i.e., $\Delta\mu_O = -1.529$ eV. (b) In the oxygen-rich conditions, oxygen partial pressure pO_2 = 1 atm, i.e., $\Delta\mu_O = -1.123$ eV.

the metal-rich and oxygen-rich conditions. For the defects with multiple site locations possible, only the lowest energy solutions are included in the plots. Below we discuss the most important defects in details.

4.1.1. Oxygen Vacancy. There are six site locations for an oxygen vacancy in layered $InGaZnO_4$ which differ by the defect's nearest-neighbor cations. A detailed comparison of the defect formation energies and its distribution in the $InGaZnO_4$ lattice is given elsewhere.[59] Specifically, it is found that the oxygen vacancy avoids Ga neighbors: the formation energy of the defect increases from 1.4 to 1.6 eV and further to 1.7 eV as the number of Ga neighbors increases from one to two and to three, respectively. However, owing to a large atomic relaxation near the defect and the formation of stable fourfold structures for both Zn and Ga, the difference in the formation energies of the oxygen defect in the $InO_{1.5}$ and $GaZnO_{2.5}$ layers is negligible, namely, 0.05 eV. Therefore, one can expect similar vacancy concentrations in the two structurally distinct layers of $InGaZnO_4$. The obtained uniform distribution of the oxygen defect throughout the layered structure of $InGaZnO_4$ contradicts with the observed anisotropy of the electrical properties in this material. Indeed, oxygen vacancies are scarce in equilibrium-grown $InGaZnO_4$, as shown below.

4.1.2. Cation Vacancies. We find that for the Fermi level above ~1.5 eV, the formation energy of the metal vacancies (the electron "killer" defects) is lower than that of the oxygen vacancy (Figure 2); hence, no conduction electrons could be produced by the oxygen defect owing to the charge compensation.

Strikingly, the cation vacancies in $InGaZnO_4$ have much lower formation energies than those in the corresponding constituent binary oxides.[22] We believe that this difference originates from a greater ability of the multicomponent lattice to adjust to the defect owing to the following factors: (i) the close proximity of several cations of different ionic radius, valence and metal−oxygen strength; (ii) the unusual five-fold coordination of Ga and Zn with the oxygen atoms; and (iii) the larger metal−oxygen distances for all cations in $InGaZnO_4$ as compared to those in the corresponding ground-phase binary oxides.[52] A cation removal may result in an energy gain once the strained metal−oxygen distances in the vicinity of the defect relax toward the regular distances making the corresponding metal−oxygen bonds stronger. As a result, the formation energy of the defect is reduced.

To verify the above assumption, we compare the defect formation energies in $InGaZnO_4$ and In_2O_3 before the atomic relaxation; these values account only for breaking the six In−O bonds in both oxides. We find that the unrelaxed formation energies of the neutral In vacancy are similar, namely, 10.5 eV in In_2O_3 and 10.3 eV in $InGaZnO_4$ under the *extreme* metal-rich conditions ($\Delta\mu_{In} = 0$). After performing full geometry optimization, the formation energy of V_{In} in $InGaZnO_4$ reduces to 8.9 eV (note, the value is for $\Delta\mu_{In} = 0$). Thus, the relaxation effect lowers the formation energy by 1.4 eV in $InGaZnO_4$. In marked contrast, the formation energy reduces by only 0.8 eV after the atomic relaxation in In_2O_3. Accordingly, we find a notably smaller atomic relaxation around V_{In} in the binary oxide (5−12%) as compared to that in $InGaZnO_4$ (10−17%). The stronger relaxation of the oxygen atoms around the V_{In} which move away from the defect and toward the next-neighbor Ga and Zn atoms (for the reasons described in the previous paragraph), results in lower formation energy of the cation vacancy defect in the multicomponent oxide.

As discussed below, in the equilibrium-grown $InGaZnO_4$, indium vacancies form at large concentrations (up to 10^{21} cm^{-3} for the oxygen partial pressure above 10^{-4} atm), whereas the gallium and zinc vacancies have lower concentrations, namely, 10^{18} cm^{-3} and below 10^{17} cm^{-3}, respectively.

4.1.3. Cation Antisites. In order to explain the conductivity in undoped $InGaZnO_4$, other electron donors beyond the oxygen vacancy and metal interstitials must be considered. Those include cation antisite defects, In^{3+} or Ga^{3+} on Zn^{2+} site. We find that both have lower formation energy than the oxygen vacancy by more than 2 eV (Figure 2), which establishes the antisite defects as the major carrier source in $InGaZnO_4$.

This result differs from the defect chemistry in Ga-free $In_2O_3(ZnO)_3$ where the calculated formation energies of In_{Zn} and V_O are comparable near the conduction band.[39] We believe that such a low formation energy of the oxygen vacancy in $In_2O_3(ZnO)_3$ arises from a larger variety of oxygen coordinations in this compound where there are six- and five-fold-coordinated In as well as five- and four-fold-coordinated Zn. In contrast, each cation in $InGaZnO_4$ has only one oxygen coordination: six-fold In and five-fold Zn or Ga. A greater freedom for the atomic relaxation around an oxygen vacancy in $In_2O_3(ZnO)_3$ leads to an additional energy gain and, hence, to a lower defect formation energy in this material. Indeed, the formation energy of the neutral oxygen vacancies at various sites in $In_2O_3(ZnO)_3$ varies over a wide range (0.2−1.4 eV in metal-rich conditions with T = 1573 K and pO_2 = 0.0001 atm), whereas in $InGaZnO_4$, the range is notably narrower (1.6−1.9 eV calculated at the same growth conditions). One can also note that the V_O formation energy in $In_2O_3(ZnO)_3$ is significantly lower than that in the corresponding binary oxides.[22] This supports our conclusion on the important role of atomic relaxation in the defect formation in multicomponent oxides.

We also find that the donor Ga_{Zn} antisite has lower formation energy as compared to In_{Zn} (Figure 2). Indeed, one can expect

dx.doi.org/10.1021/ja311955g | J. Am. Chem. Soc. 2013, 135, 5685−5692

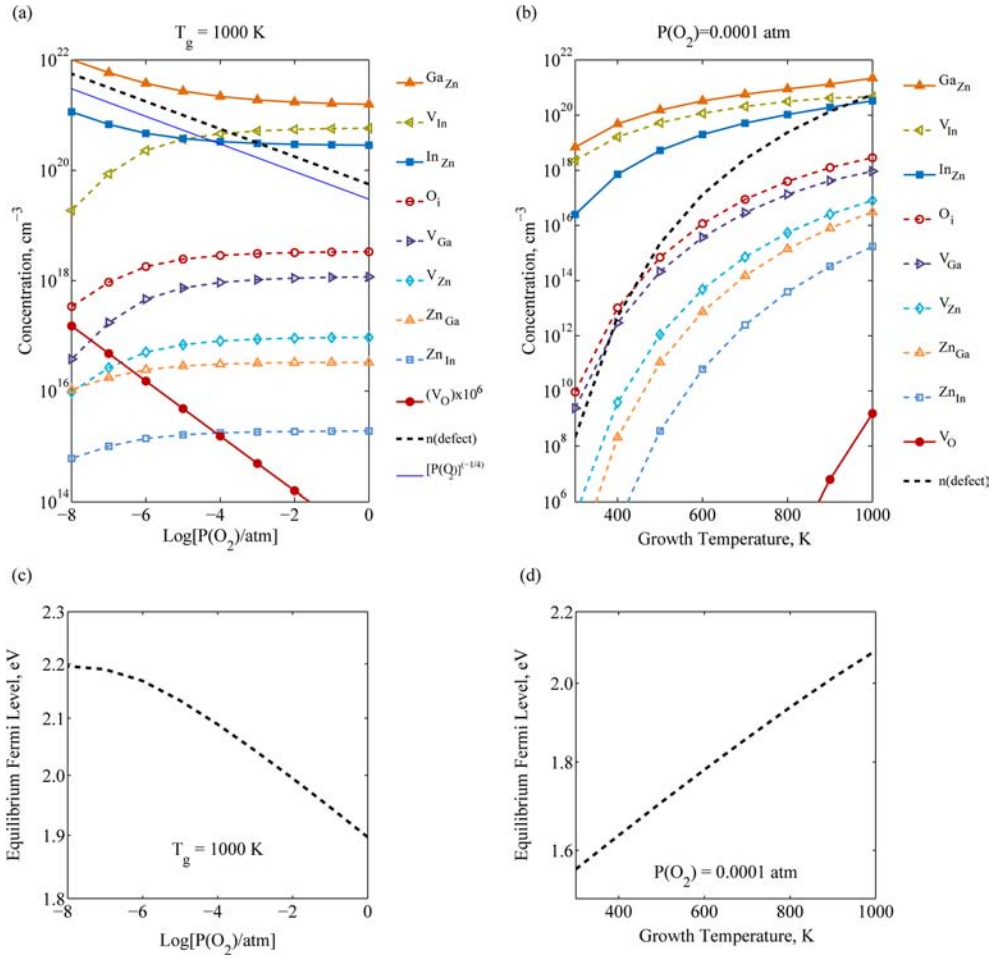

Figure 3. Calculated defect and electron (n) densities in equilibrium-grown undoped $InGaZnO_4$ (a) as a function of oxygen partial pressure pO_2 at the growth temperature 1000 K and (b) as a function of growth temperature at the oxygen pressure pO_2 = 0.0001 atm. (c,d) Corresponding pressure and growth-temperature dependence of the equilibrium Fermi level, respectively.

that the In atoms are less likely to adopt the five-fold oxygen coordination of the $GaZnO_{2.5}$ layer as compared to the "native" Ga atoms. In addition, formation of stronger Ga−O bonds in the case of Ga_{Zn} is preferred over formation of weaker In−O bonds in the case of In_{Zn}.

Further, the results for the acceptor antisites show that the formation energy of donor Ga_{Zn} is significantly lower than that of acceptor Zn_{Ga}, although both defects share the same structural layer, $GaZnO_{2.5}$, so both are in similar oxygen environments. This finding can be explained on the basis of the relative heat of formation of the corresponding binary oxides,[60,61] i.e., on the different strength of the metal−oxygen bonds which results in different energy gain/loss upon the defect formation. Specifically, in the case of the Ga_{Zn} defect, it requires less energy to break weaker Zn−O bonds; at the same time, it provides an energy gain for creating stronger Ga−O bonds. In contrast, for the Zn_{Ga} defect, more energy is needed to break the strong Ga−O bonds and little energy is gained for the creation of weak Zn−O bonds.

Comparing the formation energies of the two acceptor antisite defects, we believe that Zn_{In} has higher formation energy as compared to Zn_{Ga} due to the fact that the structure with six-coordinated Zn (rocksalt ZnO) is unstable. Both acceptor antisites have a higher formation energy compared to those of the cation vacancy defects, hence, are not significant players in the carrier generation.

4.1.4. Donor−Acceptor Complex. We also investigated the formation of $(Ga_{Zn}V_{In})$ complex. There are two site locations for Ga_{Zn} in the $GaZnO_{2.5}$ double layer with respect to the indium vacancy: one in the adjacent layer to the $InO_{1.5}$, and the other in the next $GaZnO_{2.5}$ layer, farther away from the V_{In}. We find that the energy difference between the two defects being next to each other (at the distance of about 3.6 Å) and farther away (at about 4.8 Å) is only 0.08 eV. This suggests that the interaction between the donor Ga_{Zn} and acceptor V_{In} is very weak. Indeed, since the Ga and Zn distribution in the $GaZnO_{2.5}$ layer is random, the indium vacancy is always surrounded by a mixture of Ga and Zn neighbors and, hence, experiences only a weak attraction with an additional Ga that occupies one of the Zn sites.

4.1.5. Equilibrium Defect and Carrier Concentrations. By taking into account all the defects and their possible charge states, we determine the temperature and pressure dependence of the defect concentrations in the equilibrium-grown $InGaZnO_4$. For this, the equilibrium Fermi level at each value of T and pO_2 is calculated self-consistently with the requirement of overall charge neutrality, i.e., the concentrations of carriers and all ionized defects were taken into account.[22,53] The results, presented in Figure 3, reveal that antisite Ga_{Zn} is the most abundant donor defect which determines the carrier density under the oxygen-poor conditions, specifically, for $pO_2 < 10^{-4}$ atm and growth temperature of 1000 K. As the oxygen

dx.doi.org/10.1021/ja311955g | J. Am. Chem. Soc. 2013, 135, 5685−5692

pressure increases, the electron donor is compensated by the V_{In} acceptor. The resulting equilibrium electron density follows a $(pO_2)^{-1/4}$ dependence over the experimental range of the oxygen partial pressures—in excellent agreement with our observations, as discussed below.

5. EXPERIMENTAL RESULTS

The *in situ*/equilibrium electrical properties (conductivity and Seebeck coefficient) are shown in Figure 4. To convert back to raw thermopower values, the data can be multiplied by $2.303(k/e)$ as per eq 14. Before addressing Brouwer analysis, it can be observed that both properties are consistent with the n-type character of $InGaZnO_4$, namely the negative slope of the conductivity log−log plot and the negative sign of the Seebeck coefficient. This confirms electrons as the majority electronic species at 750 °C. The fact that the two slopes (conductivity, modified Seebeck coefficient) are identical supports the assumptions necessary for Brouwer analysis, i.e., that the effective density of states, the electron mobility, and the thermopower transport term (eq 13) are essentially invariant with p_{O_2} (and carrier content) over the narrow range of experimental conditions.

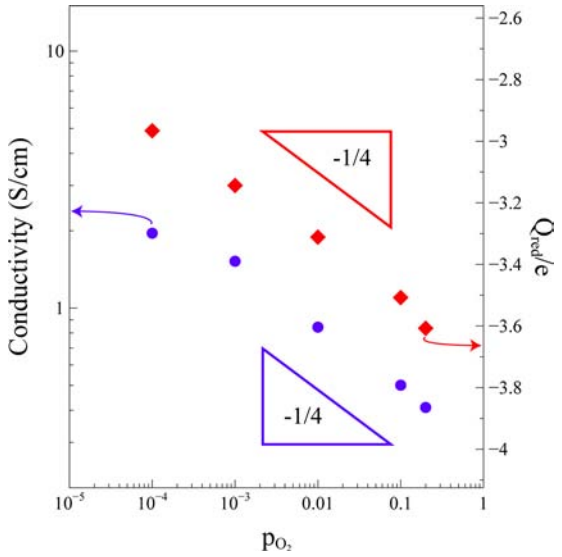

Figure 4. Dependence of $\log(\sigma)$ vs $\log(pO_2)$ and of Q_{red}/e vs $\log(pO_2)$, both supporting a −1/4 Brouwer slope which agrees well with the theoretical predictions in Figure 2.

It can also be observed from Figure 4 that the slope observed for both properties (−1/4) is inconsistent with the commonly proposed doubly charged oxygen vacancy mechanism, which would yield a (−1/6) slope. This can be illustrated from a Kröger−Vink approach, for which the defect reaction and mass-action relationship are as follows:

$$O_O^{\times} \rightleftharpoons \frac{1}{2}O_2(g) + V_O^{\bullet\bullet} + 2e' \tag{16}$$

$$(pO_2)^{-1/2}K_{V_O^{\bullet\bullet}} = [V_O^{\bullet\bullet}]n^2 \tag{17}$$

Under the electroneutrality assumption, $n = 2[V_O^{\bullet\bullet}]$, this leads to the prediction that $n \propto (pO_2)^{-1/6}$, which is clearly not observed in Figure 4.

The obtained −1/4 slope of both electrical properties is in excellent agreement with the theoretical predictions in Figure 3. From a Kröger-Vink perspective, it is relatively easy to rationalize the observed −1/4 Brouwer slope in both conductivity and reduced Seebeck coefficient. If we consider the In_2O_3 component of the structure, we can write the following point defect reaction:

$$2V_{In}''' + 3O_O^{\times} \rightleftharpoons \frac{3}{2}O_2(g) + 6e' \tag{18}$$

for which the mass-action relationship would be

$$[V_{In}''']^2 K_{red}(pO_2)^{-3/2} = n^6 \tag{19}$$

Assuming that the indium vacancy concentration is fixed by the Ga_{Zn} antisite population ($[V_{In}'''] = (1/3)[Ga_{Zn}^{\bullet}]$) as shown by theory at high pO_2 values (Figure 3), we arrive at

$$n = (\text{Const.})^{1/6}(pO_2)^{-1/4} \tag{20}$$

resulting in the slopes observed in Figure 4.

It should be stressed that, under these conditions, electrons are a minority species (to $[V_{In}''']$ and $[Ga_{Zn}^{\bullet}]$).

5.1. Conductivity Behavior in In-Rich vs Ga-Rich $InGaZnO_4$. The above findings also help understand earlier observations in $InGaZnO_4$ with variable In:Ga ratio.[26] In particular, it was observed that the conductivity drops significantly in the Ga-rich case and increases rather moderately in the In-rich case. Based on the defect chemistry obtained for $InGaZnO_4$, we explain the conductivity behavior as follows. In the Ga-rich/In-poor case, a larger concentration of Ga_{Zn} antisites is expected. However, the defect is abundant already for the 1:1 ratio of Ga to In (we obtained 2×10^{21} cm^{-3} or higher, Figure 3), and an increase in Ga:In ratio from 1:1 may result in overdoping and disrupt the stability of the $n = 1$ phase. Indeed, this is consistent with experimental observations that there is only a limited solubility of additional Ga (an increase in Ga:In ratio) in $InGaZnO_4$.[26,62] At the same time, increasing the Ga:In ratio increases the concentration of the electron killer V_{In} that leads to a strong compensation of the electron donor and pushes the equilibrium Fermi level farther away from the conduction band edge deeper into the band gap. Therefore, the conductivity decreases rapidly in the Ga-rich/In-poor case. On the other hand, when the In:Ga ratio is increased (i.e., in Ga-poor/In-rich growing conditions for $InGaZnO_4$), the additional In suppresses the amount of the detrimental In vacancies. The conductivity, however, increases only moderately, although steadily—owing to the limited formation of the Ga_{Zn} antisites in this Ga-poor case and as the In_{Zn} antisites become more pronounced under the In-rich conditions and contribute to the overall number of the electron carriers.

6. CONCLUSIONS

In summary, thorough theoretical and experimental investigations help explain the carrier generation and transport in crystalline $InGaZnO_4$. The observed dependence of the conductivity and the calculated dependence of the carrier density on the oxygen partial pressure, $\sigma \sim n \sim (pO_2)^{-1/4}$, rules out the oxygen vacancy as a carrier source in crystalline $InGaZnO_4$, as it was commonly accepted for a decade. Accurate calculations of the formation energy of possible acceptor and donor defects in $InGaZnO_4$ reveal that the major electron donor is the cation antisite Ga_{Zn}, which is strongly compensated by the V_{In} acceptor for the oxygen partial pressure $pO_2 > 10^{-4}$ atm. Owing to the random distribution of the Ga and Zn atoms in the mixed $GaZnO_{2.5}$ layer, the

dx.doi.org/10.1021/ja311955g | J. Am. Chem. Soc. 2013, 135, 5685−5692

interaction between the major donor and most abundant acceptor is weak, i.e., the formation of the $(Ga_{Zn}V_{In})$ complex is unlikely.

The proposed carrier generation mechanism in undoped $InGaZnO_4$ also helps explain the intriguing conductivity behavior in the multicomponent oxide grown under In-rich or Ga-rich conditions, i.e., when the In:Ga ratio varies from 1:1.

Finally, we show that the acceptor and donor defect formation and distribution in multicomponent oxides is strongly affected not only by the chemical composition but also by the local oxygen coordination and by the ability of the multicomponent lattice to adjust to the new environment created by the defect via relaxation. Such an in-depth understanding of the complex defect chemistry is instructive in guiding future search for candidates with a set of optical and electronic properties that can be controlled by variation in the crystal structure, chemical composition and carrier generation mechanisms.

AUTHOR INFORMATION

Corresponding Author

juliaem@mst.edu

Notes

The authors declare no competing financial interest.

ACKNOWLEDGMENTS

This work was performed under the collaborative MRSEC program at Northwestern University and supported by the National Science Foundation (NSF) grant DMR-1121262. A.M. was also partially supported by NSF grant DMR-0705626. Computational resources are provided by the NSF-supported TeraGrid/XSEDE program.

REFERENCES

(1) Vossen, J. *Physics of Thin Films*; Academic Press: New York, 1977; Vol. *9*, pp 1−71.
(2) Chopra, K. L.; Major, S.; Pandya, D. K. *Thin Solid Films* **1983**, *102*, 1.
(3) Dawar, A. L.; Joshi, J. C. *J. Mater. Sci.* **1984**, *19*, 1.
(4) Hartnagel, H. L.; Dawar, A. L.; Jain, A. K.; Jagadish, C. *Semiconducting Transparent Thin Films*; Institute of Physics Publishing: London, 1995.
(5) Ginley, D. S.; Bright, C. *MRS Bull.* **2000**, *25*, 15.
(6) Ingram, B. J.; Gonzalez, G. B.; Kammler, D. R.; Bertoni, M. I.; Mason, T. O. *J. Electroceram.* **2004**, *13*, 167.
(7) Edwards, P. P.; Porch, A.; Jones, M. O.; Morgan, D. V.; Perks, R. M. *Dalton Trans.* **2004**, *19*, 2995.
(8) Exarhos, G. J.; Zhou, X.-D. *Thin Solid Films* **2007**, *515*, 7025.
(9) Fortunato, E.; Ginley, D.; Hosono, H.; Paine, D. C. *MRS Bull.* **2007**, *32*, 242.
(10) Facchetti, A.; Marks, T. *Transparent Electronics: From Synthesis to Applications*; John Wiley & Sons: New York, 2010.
(11) Ginley, D. S.; Hosono, H.; Paine, D. C. *Handbook of Transparent Conductors*; Springer: Berlin, 2011.
(12) Frank, G.; Köstlin, H. *Appl. Phys. A: Mater. Sci. Process.* **1982**, *27*, 197.
(13) González, G. B.; Cohen, J.; Hwang, J.; Mason, T.; Hodges, J.; Jorgensen, J. *J. Appl. Phys.* **2001**, *89*, 2550.
(14) Mryasov, O. N.; Freeman, A. J. *Phys. Rev. B* **2001**, *64*, 233111.
(15) Kiliç, Ç.; Zunger, A. *Phys. Rev. Lett.* **2002**, *88*, 95501.
(16) de Walle, C. G. V. *Phys. Stat. Solidi B* **2002**, *229*, 221.
(17) Tanaka, I.; Tatsumi, K.; Nakano, M.; Adachi, H. *J. Am. Ceram. Soc* **2002**, *85*, 68.
(18) Mizoguchi, H.; Woodward, P. M. *Chem. Mater.* **2004**, *16*, 5233.
(19) Robertson, J. *Thin Solid Films* **2008**, *516*, 1419.
(20) Medvedeva, J. E.; Freeman, A. J. *Europhys. Lett.* **2005**, *69*, 583.
(21) Medvedeva, J. E. *Appl. Phys. A: Mater. Sci. Process.* **2007**, *89*, 43.
(22) Lany, S.; Zunger, A. *Phys. Rev. Lett.* **2007**, *98*, 045501.
(23) González, G.; Mason, T.; Quintana, J.; Warschkow, O.; Ellis, D.; Hwang, J.-H.; Hodges, J.; Jorgensen, J. *J. Appl. Phys.* **2004**, *96*, 3912.
(24) Orita, M.; Takeuchi, M.; Sakai, H.; Tanji, H. *Jpn. J. Appl. Phys.* **1995**, *34*, L1550.
(25) Hiramatsu, H.; Seo, W. S.; Koumoto, K. J. *Chem. Mater.* **1998**, *10*, 3033.
(26) Moriga, T.; Kammler, D.; Mason, T.; Palmer, G.; Poeppelmeier, K. *J. Am. Ceram. Soc.* **1999**, *82*, 2705.
(27) Freeman, A. J.; Poeppelmeier, K. R.; Mason, T. O.; Chang, R. P.; Marks, T. J. *MRS Bull.* **2000**, *25*, 45.
(28) Orita, M.; Ohta, H.; Hirano, M.; Narushima, S.; Hosono, H. *Philos. Mag. B* **2001**, *81*, 501.
(29) Nomura, K.; Ohta, H.; Ueda, K.; Kamiya, T.; Hirano, M.; Hosono, H. *Science* **2003**, *300*, 1269.
(30) Nomura, K.; Ohta, H.; Takagi, A.; Kamiya, T.; Hirano, M.; Hosono, H. *Nature* **2004**, *432*, 488.
(31) Hosono, H. *J. Non-Cryst. Solids* **2006**, *352*, 851.
(32) Leenheer, A. J.; Perkins, J. D.; van Hest, M. F. A. M.; Berry, J. J.; O'Hayre, R. P.; Ginley, D. S. *Phys. Rev. B* **2008**, *77*, 115215.
(33) Nomura, K.; Takagi, A.; Kamiya, T.; Ohta, H.; Hirano, M.; Hosono, H. *Jpn. J. Appl. Phys.* **2006**, *45*, 4303.
(34) Kamiya, T.; Nomura, K.; Hirano, M.; Hosono, H. *Phys. Stat. Solidi C* **2008**, *5*, 3098.
(35) Noh, H.-K.; Chang, K.; Ryu, B.; Lee, W.-J. *Phys. Rev. B* **2011**, *84*, 115205.
(36) Omura, H.; Kumomi, H.; Nomura, K.; Kamiya, T.; Hirano, M.; Hosono, H. *J. Appl. Phys.* **2009**, *105*, 093712.
(37) Medvedeva, J. E.; Hettiarachchi, C. L. *Phys. Rev. B* **2010**, *81*, 125116.
(38) Chen, C.; Cheng, K.-C.; Chagarov, E.; Kanicki, J. *Jpn. J. Appl. Phys.* **2011**, *50*, 091102.
(39) Peng, H.; Song, J.-H.; Hopper, E. M.; Zhu, Q.; Mason, T. O.; Freeman, A. J. *Chem. Mater.* **2012**, *24*, 106.
(40) Wimmer, E.; Krakauer, H.; Weinert, M.; Freeman, A. J. *Phys. Rev. B* **1981**, *24*, 864.
(41) Weinert, M.; Wimmer, E.; Freeman, A. J. *Phys. Rev. B* **1982**, *26*, 4571.
(42) Bylander, D. M.; Kleinman, L. *Phys. Rev. B* **1990**, *41*, 7868.
(43) Seidl, A.; Görling, A.; Vogl, P.; Majewski, J. A.; Levy, M. *Phys. Rev. B* **1996**, *53*, 3764.
(44) Asahi, R.; Mannstadt, W.; Freeman, A. J. *Phys. Rev. B* **1999**, *59*, 7486−7492.
(45) Geller, C. B.; Wolf, W.; Picozzi, S.; Continenza, A.; Asahi, R.; Mannstadt, W.; Freeman, A. J.; Wimmer, E. *Appl. Phys. Lett.* **2001**, *79*, 368.
(46) Kim, M. Y.; Asahi, R.; Freeman, A. J. *J. Comput.-Aided Mater. Des* **2002**, *9*, 173.
(47) Kato, V. K.; Kawada, I.; Kimizuka, N.; Katsura, T. *Z. Kristall.* **1975**, *141*, 314.
(48) Kimizuka, N.; Mohri, T. *J. Solid State Chem.* **1985**, *60*, 382.
(49) Kimizuka, N.; Mohri, T. *J. Solid State Chem.* **1989**, *78*, 98.
(50) Li, C.; Bando, Y.; Nakamura, M.; Kimizuka, M. *J. Electron Microsc.* **1997**, *46*, 119.
(51) Medvedeva, J. E. *Europhys. Lett.* **2007**, *78*, 57004.
(52) Murat, A.; Medvedeva, J. E. *Phys. Rev. B* **2012**, *85*, 155101.
(53) Osorio-Guillén, J.; Lany, S.; Barabash, S. V.; Zunger, A. *Phys. Rev. Lett.* **2006**, *96*, 107203.
(54) Lany, S.; Zunger, A. *Phys. Rev. B* **2008**, *78*, 235104.
(55) Choy, T. *Effective Medium Theory*; Clarendon Press: Oxford, 1999.
(56) McLachlan, D.; Blaszkiewicz, M.; Newnham, R. *J. Am. Ceram. Soc.* **1990**, *73*, 2187.
(57) Bruggeman, D. A. G. *Ann. Phys.* **1935**, *416*, 636.
(58) Hong, B.; Ford, S.; Mason, T. *Key Eng. Mater.* **1996**, *6*, 163.
(59) Murat, A.; Medvedeva, J. E. *Phys. Rev. B* **2012**, *86*, 085123.

(60) Reed, T. B. *Free energy of formation of binary compounds*; MIT Press: Cambridge, MA, 1971.
(61) Dean, J., Ed. *Lange's Handbook of Chemistry*; McGraw-Hill: New York, 1999.
(62) Nakamura, N. K. M.; Mohri, T. *J. Solid State Chem.* **1991**, *93*, 298.